Available online at www.sciencedirect.com

SciVerse ScienceDirect

Nuclear Physics A 873 (2012) 17–27

NUCLEAR PHYSICS A

www.elsevier.com/locate/nuclphysa

Breakup coupling effects on near-barrier inelastic scattering of the weakly bound ^{6}Li projectile on a ^{144}Sm target

A.E. Woodard [a,*,1], J.M. Figueira [a,b], D.R. Otomar [c], J.O. Fernández Niello [a,b,d], J. Lubian [c], A. Arazi [a,b], O.A. Capurro [a], P. Carnelli [a,b], L. Fimiani [a], G.V. Martí [a], D. Martinez Heimann [a,b], D.S. Monteiro [c], A.E. Negri [a], A.J. Pacheco [a,b], P.R.S. Gomes [c]

[a] *Laboratorio Tandar, Comisión Nacional de Energía Atómica, B1650KNA San Martín, Buenos Aires, Argentina*
[b] *Consejo Nacional de Investigaciones Científicas y Técnicas, C1033AAJ Ciudad de Buenos Aires, Argentina*
[c] *Instituto de Física, Universidade Federal Fluminense, Gragoatá, Niterói, R. J., 24210-340, Brazil*
[d] *Escuela de Ciencia y Tecnología, Universidad de San Martín, B1650BWA San Martín, Buenos Aires, Argentina*

Received 8 August 2011; received in revised form 1 October 2011; accepted 10 October 2011

Available online 21 October 2011

Abstract

Angular distributions for the inelastic scattering of the weakly bound ^{6}Li nucleus from a ^{144}Sm target (associated with the contributions of both the 2_1^+ and 3_1^- ^{144}Sm excited states together) were measured at bombarding energies close to the Coulomb barrier. The experimental data were compared with expected results based on continuum discretized coupled-channel (CDCC) calculations. The results confirm that it is essential to include continuum–continuum couplings to reproduce the experimental data. The analysis demonstrates that inelastic scattering data can be a critical tool in testing full CDCC calculations involving weakly bound nuclei.

Keywords: NUCLEAR REACTIONS ^{144}Sm(^{6}Li,^{6}Li), $E = 23.0$–35.1 MeV; measured scattered ^{6}Li spectra using surface barrier detector array; deduced $\sigma(\theta)$ for different target excitations, reaction mechanism features. Comparison with continuum discretized coupled-channel calculations

* Corresponding author.
E-mail address: awoodard@nd.edu (A.E. Woodard).
[1] Present address: Physics Department, University of Notre Dame, Notre Dame, IN 46556, USA.

0375-9474/$ – see front matter
doi:10.1016/j.nuclphysa.2011.10.003

1. Introduction

The effect of breakup of weakly bound systems on different reaction mechanisms and scattering has been extensively studied [1]. However, both theoretical and experimental results have been inconsistent in some areas, and consequently this effect is still not fully understood. Recently, our group has investigated the influence of breakup on the ^{6}Li + ^{144}Sm system at incident energies near the Coulomb barrier by different forms: backward angle quasi-elastic scattering and the corresponding barrier distribution (QEBD) [2,3], elastic scattering [4,5] and exclusive measurements of the emitted d and α particle in the breakup process [6,7]. ^{6}Li is a weakly bound projectile with breakup threshold energy of 1.67 MeV and no bound excited states, while ^{144}Sm is a nearly spherical target. In Ref. [4], experimental elastic scattering angular distributions were presented for near-barrier energies, and the energy dependence of the optical potential was investigated. In a later theoretical work [5], those experimental angular distributions were studied by means of continuum discretized coupled-channel (CDCC) calculations. In addition to the elastic scattering angular distributions reported in Ref. [4], the inelastic scattering leading to the combined 2_1^+ ($E^* = 1.66$ MeV) and 3_1^- ($E^* = 1.81$ MeV) target excited states was also measured in this experiment. In the present paper we report those inelastic scattering data and their analysis by means of CDCC calculations. The goal is to reproduce simultaneously both elastic and inelastic scattering as a stringent proof of the proposed model. In this way, we investigate the effect of breakup on the inelastic scattering angular distributions.

2. Experimental setup

The experimental details have been reported previously in Ref. [4], and are summarized briefly here. The beam of ^{6}Li was produced in the 20 UD tandem accelerator at the TANDAR Laboratory in Buenos Aires. The bombarding energy of the projectile was varied around the Coulomb barrier ($V_b^{lab} = 24.5$ MeV) between 23.0 and 35.1 MeV. The ^{144}Sm target had 120 μg/cm^2 of thickness, enriched to 88% and it was evaporated onto 20 μg/cm^2 of carbon backing. An array of eight surface-barrier detectors was used, with an energy resolution ranging from 0.5% to 1.0%. The angular distributions were measured in steps of 2.5° or 5.0°. They are reported in the angular range from 40° to 170°, where it is possible to distinguish between events associated with the inelastic scattering from the ^{144}Sm target and the elastic scattering from the target contaminations (^{16}O) and ^{12}C in the backing film. Fig. 1 shows typical spectra measured at $E_{lab} = 23.0$ MeV and $\theta_{\text{c.m.}} = 127.3°$ and $E_{lab} = 28.0$ MeV and $\theta_{\text{c.m.}} = 124.6°$. The inelastic excitations of the target are marked in the figure by arrows. For most of the spectra, it was not possible to separate the 2_1^+ and 3_1^- ^{144}Sm states. Consequently the inelastic angular distributions we report are the sum of the cross sections of these two excited states. The statistical uncertainty of the cross sections ranges from 10% to 50%.

3. CDCC model space

At present, the most successful method to deal with the complexity of coupling continuum states among them and with the bound states is the CDCC method [8,9]. Within this method, the scattering states are grouped into wave packets or bins with defined angular momenta, to obtain representative bin wave functions that belong to the Hilbert space. Hence they give non-infinite matrix elements when the interaction potential is folded between these bin states. With this approach the continuum states can be coupled as if they were "inelastic excitations", but with a

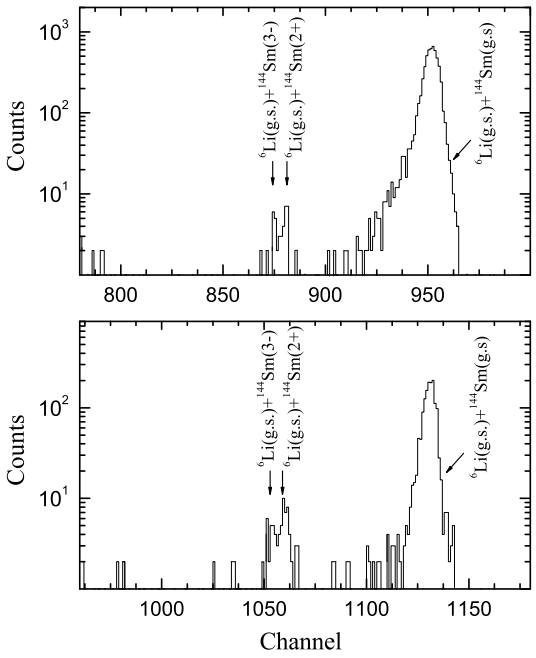

Fig. 1. Energy spectra of the reaction products around the elastic peak for the ^{6}Li + ^{144}Sm system, measured at $E_{lab} = 23$ MeV and $\theta_{\mathrm{c.m.}} = 127.3°$ (top), and $E_{lab} = 28$ MeV and $\theta_{\mathrm{c.m.}} = 124.6°$ (bottom). Different exit channels are indicated.

model space considerably larger than the one that includes only bound states. The coupled channel calculation has an infinite configuration space, which must be truncated without excluding the states of interest. For this reason, calculating the numerical solution by means of the CDCC method can be difficult and must include rigorous tests of convergence.

The wave function of the system with total angular momentum J and z-projection M can be schematically written as

$$\Psi^{JM}(\mathbf{R}, \mathbf{r}, \xi) = \sum_{\mathrm{i}} \frac{F_{\mathrm{i}}^{J}(\mathrm{R})}{\mathrm{R}} \mathcal{Y}_{\mathrm{i}}^{JM}(\hat{\mathbf{R}}, \mathbf{r}, \xi). \tag{1}$$

In this expression, the index i stands for the set of quantum numbers $\{\varepsilon_{\mathrm{i}}, l_{\mathrm{i}}, j_{\mathrm{i}}, I_{\mathrm{i}}, L\}$ where ε is the energy at the center of the bin, l is the relative orbital angular momentum of the clusters that summed to the spin of the deuteron give the total angular momentum j, L stands for the relative projectile-target angular momentum, and I is the spin of the collective excitation of the target. The variables $\mathbf{R}$, $\mathbf{r}$ and ξ stand for the projectile-target separation vector, projectile internal coordinate and target internal degrees of freedom, respectively, and $\hat{\mathbf{R}}$ represents the angular part of the vector $\mathbf{R}$. $F_{\mathrm{i}}^{J}(\mathrm{R})$ is the radial wave function of the projectile-target relative motion while $\mathcal{Y}_{\mathrm{i}}^{JM}(\hat{\mathbf{R}}, \mathbf{r}, \xi)$ is a triple tensor product of the full internal wave functions of the target, the bins, and the angular part of the projectile-target relative motion. Using the standard procedure of integrating over all the variables except R, the following system of coupled equations is obtained

$$\left[T_L + U_{\mathrm{ii}}^{J}(\mathrm{R}) - E + \epsilon_{\mathrm{i}}\right] F_{\mathrm{i}}^{J}(\mathrm{R}) = -\sum_{\mathrm{j}} U_{\mathrm{ij}}^{J}(\mathrm{R}) F_{\mathrm{j}}^{J}(\mathrm{R}), \tag{2}$$

where the matrix elements in Eq. (2) are given by

$$U_{\mathrm{ij}}^{J}(\mathrm{R}) = \int d\hat{\mathbf{R}}\, d\mathbf{r}\, d\xi\, \mathcal{Y}_{\mathrm{i}}^{JM*}(\hat{\mathbf{R}}, \mathbf{r}, \xi) V(\mathbf{R}, \mathbf{r}, \xi) \mathcal{Y}_{\mathrm{j}}^{JM}(\hat{\mathbf{R}}, \mathbf{r}, \xi). \tag{3}$$

In the present CDCC calculation for the ^{6}Li + ^{144}Sm system, we postulate that the ^{6}Li breaks up into α-particles and deuterons and we assume that the cluster model is valid [10,11]. The only bound state of the clusters is their ground state, corresponding to the entrance channel. The projectile's remaining states within the model space are in the continuum, and it is necessary to generate a set of bins to represent them. Special care has to be taken to account for resonant states of the ^{6}Li projectile, in order to avoid double counting. The scattering optical potential used to generate the bins was the one used in Refs. [12,3,5]. The convergence of the CDCC method, as will be shown below, was reached with bins with maximum energy of $\varepsilon_{\max} = 7$ MeV in the whole energy range studied. The energy was discretized for relative orbital angular momentum of the α-deuteron clusters $l \leqslant 2$.

In order to describe the unbound resonant states, different discretizations in energy were used for different angular momenta of the cluster. For $l = 0, 1$, the discretizations were the same and resulting in 2 bins/MeV. The choice of the bins for $l = 2$ was guided to describe the resonant states. For this purpose, three different groups of bins were used for $J^{\pi} = 3^{+}, 2^{+}$ and 1^{+}, that are the unbound resonant states of the ^{6}Li projectile, obtained by coupling the $l = 2$ angular momentum plus the spin of the deuteron $s = 1$. The α-deuteron interaction potential is of Wood–Saxon form and includes the spin-orbit interaction, as described in Ref. [12]. This potential was shown to describe the experimental widths and energies of the resonant states of the projectile. For the 1^{+} and 2^{+} continuum states, 2.5 bins/MeV were taken inside the resonances. For energies below and above the resonances, 2 bins/MeV and 2.5 bins/MeV were used, respectively. For the 3^{+} continuum bins, the discretization was as follows: 7.7 bins/MeV, 10.0 bins/MeV and 7.7 bins/MeV below, inside and above the resonance, respectively. The matching radius that guaranteed the orthogonality between bins was $r_{\mathrm{bin}} = 160$ fm. The projectile-target relative motion wave functions were expanded up to $200\hbar$ in the whole energy interval and integrated up to a maximum radius of $R_{\max} = 500$ fm of the relative projectile-target distance. This was to ensure the convergence of the wave functions to the asymptotic Coulomb functions for all of the individual angular distributions. Fragment-target potentials were expanded up to the quadrupole term ($K_{\max} \leqslant 2$) because the octupole term gave negligible effects on the calculated cross sections.

To evaluate the matrix elements of Eq. (3) in the cluster model, one splits the interaction into a number of cluster terms. In the present calculations, the interaction was split into two cluster terms corresponding to the α-target interaction and deuteron-target interactions, including Coulomb and nuclear parts

$$V(\mathbf{R}, \mathbf{r}, \xi) = V_{\alpha-\mathrm{T}}(\mathbf{R}, \mathbf{r}, \xi) + V_{d-\mathrm{T}}(\mathbf{R}, \mathbf{r}, \xi). \tag{4}$$

For the real part of the nuclear potentials, a double folding type potential was used. The matter density of the ^{144}Sm target was taken from the systematic of the São Paulo potential [13]. Assuming that charge and matter densities have similar distributions, the matter density distribution of the deuteron and the ^{4}He cluster were obtained by doubling the charge distribution reported in Ref. [14]. For the imaginary parts of the optical potentials, an internal Woods–Saxon form factor was used with depth $W_0 = 50.0$ MeV, reduced radius $r_0 = 1.06$ fm and diffuseness $a = 0.2$ fm. This internal potential is equivalent to the so-called Ingoing Wave Boundary Condition and is responsible for the absorption of flux to fusion after one or both clusters has/have overcome the Coulomb barrier, representing then the total fusion cross section. In Ref. [5], it has been shown

that the cross sections are almost completely insensitive to the choice of the internal imaginary potentials, as long as they are kept internal. The main reason to keep them internal with respect to the barrier is because if the absorption potential reached the surface (the barrier region), it would account for the absorption into other direct reaction channels not included in the coupling scheme, like inelastic scattering and transfer reactions. Since these direct channels will be taken into account explicitly in our calculations, we have to avoid double counting.

In what follows we would like to briefly discuss and summarize a few points of the procedure that we have applied. It is especially important to emphasize the treatment that we have given to the inelastic excitations and the internal degrees of freedom of the target, as well as the special attention that we have paid to the possible problem that stems from double counting. Although we are not dealing in this work with the fusion cross section calculation, we would like to emphasize that while a short-range imaginary potential, acting on the projectile center-of-mass may produce a short-range absorption, it is not obvious that a short-range imaginary potential acting on the fragment-target relative coordinate will also necessarily lead to a short-range absorption in the projectile-target center of mass. In fact, if the relative separation of the fragments is large enough that the projectile is in a continuum state, then absorbing the center-of-mass of the projectile does not necessarily imply that any of the fragments will be absorbed, as is the case for the present projectile where the two breakup fragments have comparable masses. The absorption of the center-of-mass of the projectile will lead to the absorption of at least one fragment if the mass of one fragment is much larger than the other [15]. As pointed out in Eq. (4), the potential that we take is the sum of two terms corresponding to the interactions between the target and each one of the breakup fragments (alpha particle and deuteron). Our approach is based on a method that has been recently proposed to separate complete and incomplete fusion for the deuterium induced reaction within the CDCC formalism [16]. In that method, the integrations are performed over the fragment-target spatial coordinates instead of using the projectile-target and the internal projectile coordinates. Moreover, these fragment-target interactions are described in terms of bare potentials to which one needs to explicitly add the collective couplings in the usual coupled channel method, where the real parts of the interaction potentials are expanded in multipoles in order to obtain the transition form-factors. Using the harmonic vibrational model the transition matrix elements are found to lead to the same effect as the optical potential that describes the elastic scattering [17]. All calculations presented in this manuscript were performed with the code FRESCO [18]. Since the current version of the code does not include the excitation of the target in the CDCC method, all form-factors and reduced matrix elements were given as external values. In the present calculation the potential that is deformed to describe the inelastic excitations of the target is obtained by single folding the sum of the fragment-target potentials and the projectile ground state wave function. The extension of the CDCC method to include target excitations has been performed in a limited number of works (see for example a work of Yahiro et al. [19]). Recently, there have also been some works which take into account the excitation of the core if the projectile is considered as a core plus a valence particle [20].

In the present calculation, neither the excitations of the α-core nor those of the deuteron internal degrees of freedom are included in the coupling scheme. A possible sequential breakup of the deuteron was also not included in the calculations. As mentioned before, besides the excitation of the continuum states of the projectile, the collective internal degrees of freedom of the ^{144}Sm target are included in the calculations. The corresponding channels are labeled by the values of the target's intrinsic angular momentum I. Deformation parameters of $\beta_2 = 0.087$ [21] and $\beta_3 = 0.130$ [22] were used for the 2_1^+ and 3_1^- ^{144}Sm excited states, respectively. Simultaneous excitations of the projectile and the target were not considered. It is important to point out here

that our calculations do not employ any fitting procedure, using free parameters in order to obtain the best adjustment to the inelastic angular distributions.

4. Results and discussion

Fig. 2 compares the experimental inelastic scattering angular distributions at $E_{lab} = 23.0, 24.1, 26.0, 28.0, 30.1, 32.2$ and 35.1 MeV to different theoretical approaches. The solid curves represent the full CDCC calculation including all reorientation terms of the continuum couplings, including the continuum–continuum couplings as well as the inelastic excitations of the ^{144}Sm target. The experimental data are generally consistent with the model but exceed the predicted values at the lowest energies. Although the results of the calculations are sensitive to small variations in the value of the deformation parameter β_2 used for the ^{144}Sm target, variations of this parameter by up to 10% does not significantly improve the agreement between the model and the data. The dashed curves represent the usual CC calculations (where the breakup channel is not considered) using the interaction of the whole projectile with the target, with the matter density for the ^{6}Li projectile taken from the São Paulo potential systematic. For the highest energies it can be seen that this CC calculation over-predicts the experimental data and does not reproduce the shape of the inelastic angular distributions. In Fig. 2 we also show the effect of the continuum–continuum coupling (CCC) in the CDCC calculations for the inelastic scattering. The dotted curves are the results of CDCC calculations when the CCC are not included, that is, when all the matrix elements given in Eq. (3) which do not couple the ^{6}Li ground state with any bin wave function are taken equal to zero. By comparing the full CDCC calculations to those without CCC, one can observe that at near-barrier energies the effect of the CCC on the inelastic scattering angular distributions is negligible. However, its importance increases noticeably for higher energies. The effect of taking into account the CCC is to increase the inelastic cross sections. A similar effect was reported for elastic scattering angular distributions calculated for the ^{8}B + ^{58}Ni system at near-barrier energies [23,24]. In Ref. [24] it was shown that the reason for the enhancement of the elastic cross section was the real repulsive dynamic polarization potential due to CCC and the reduction of its long range absorptive imaginary part, related to the breakup channel. The real repulsive dynamic polarization potential increases the Coulomb barrier and consequently reduces the fusion probability. The loss of flux going to fusion feeds the peripheral channels, like elastic and inelastic scattering and other direct reactions. In spite of the small discrepancies discussed above, we conclude that when the breakup channel is present the best description of the data is obtained performing a full CDCC calculation that contains all important channels in the coupling scheme, including continuum–continuum couplings. Some previous reports [2,3,25–27] have analyzed backscattering quasi-elastic barrier distributions (QEBD) using CC calculations for weakly bound systems and have reached conclusions concerning the importance of the role played by inelastic or transfer channels without explicitly considering the breakup channel. It may be necessary to revise these conclusions, considering that the most striking differences between full CDCC and the usual CC calculations are precisely at the largest angles.

In Fig. 3 we compare the results of the full CDCC calculations to the elastic scattering angular distributions. This comparison has already been reported [5], but here it is enlarged to show the low energies in detail. It can be seen that there is also some disagreement between calculations and experimental data at low energies. For the elastic scattering, the calculations over-predict the data, while for inelastic scattering the data are greater than predicted. It is very important to stress that the disagreement between the calculations and the experimental data is much more evident

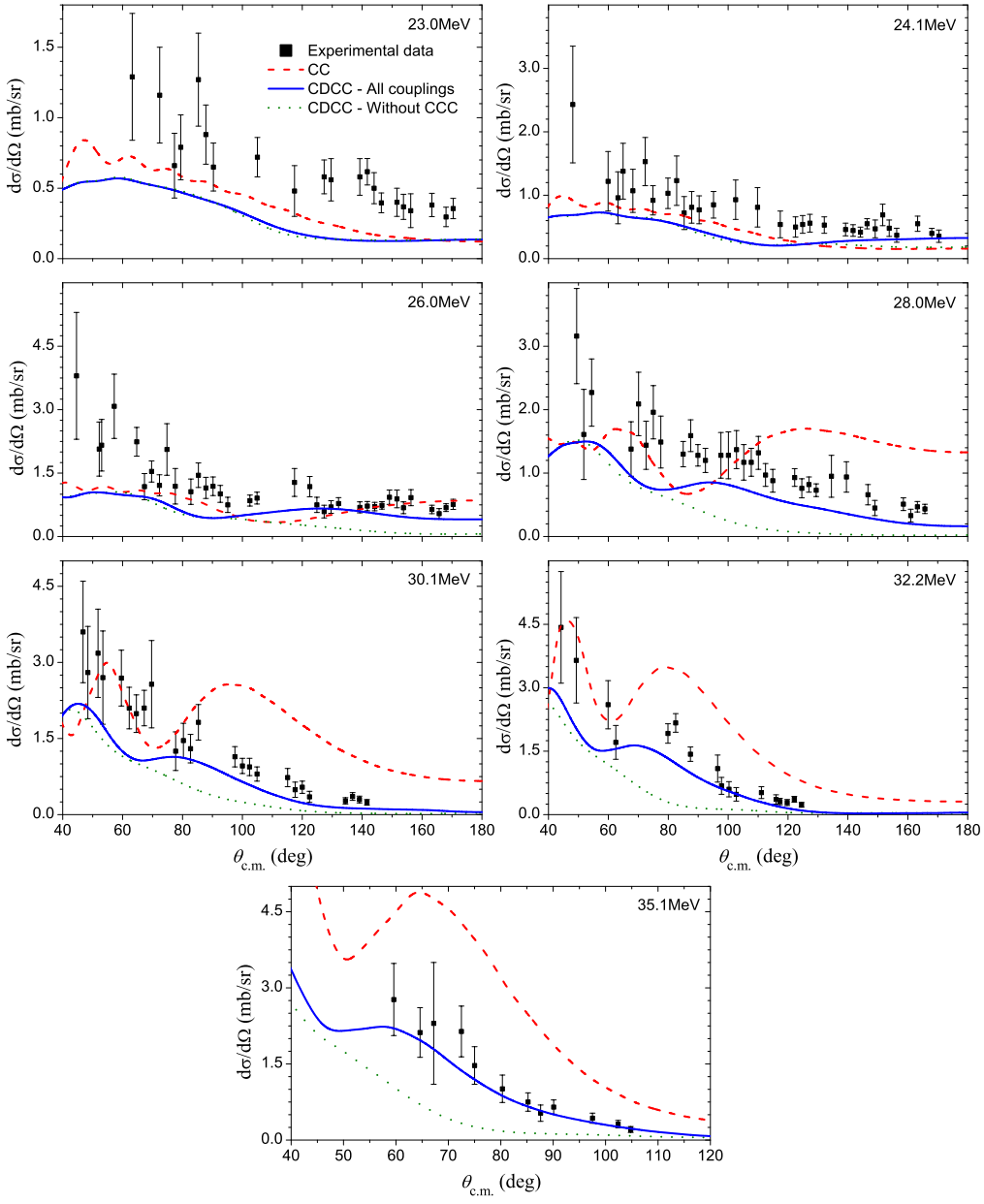

Fig. 2. (Color online.) Experimental and calculated angular distributions of inelastic scattering cross sections of the weakly bound ^{6}Li nucleus from a ^{144}Sm target, with contribution from the 2_1^+ and the 3_1^- target excited states at $E_{lab} = 23.0, 24.1, 26.0, 28.0, 30.1, 32.2$ and 35.1 MeV. Different calculations correspond to: full CDCC calculation including all reorientation terms of the continuum couplings, the continuum–continuum couplings as well as the inelastic excitations of the ^{144}Sm target (solid curves), the usual CC calculation that does not take into account the breakup channel (dashed curves), and the results of CDCC calculations when the continuum–continuum couplings are switched off (dotted curves).

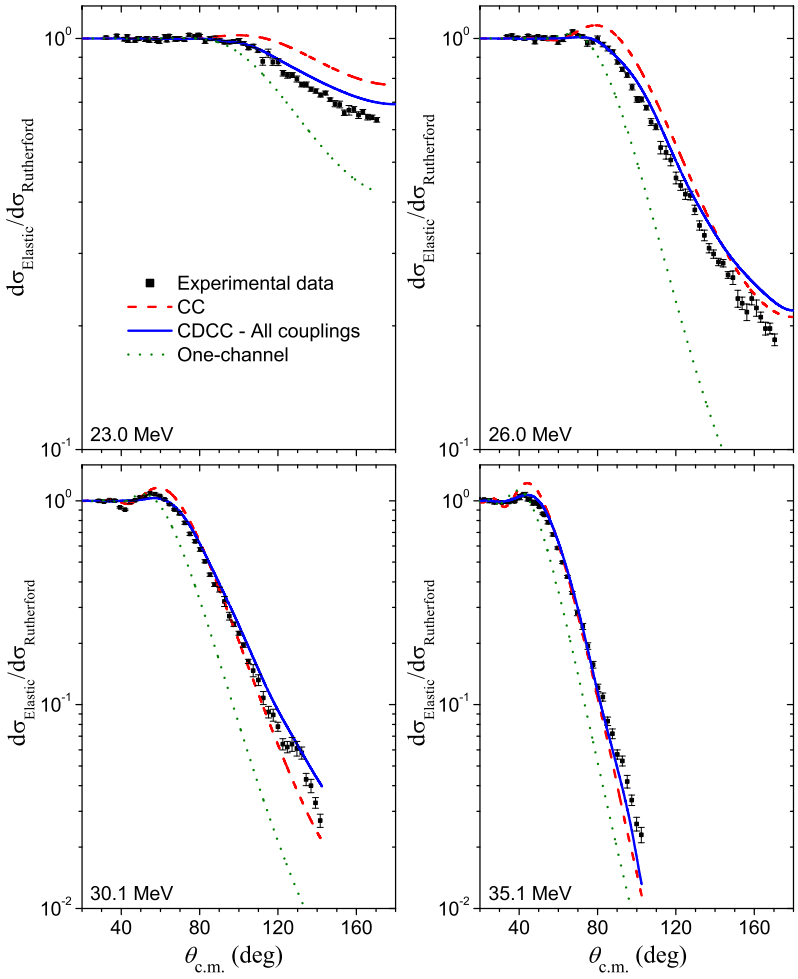

Fig. 3. (Color online.) Comparison between experimental and calculated elastic scattering angular distributions for the ^{6}Li + ^{144}Sm system. The experimental data were taken from Ref. [4] and normalized to the Rutherford cross section. Different calculations correspond to: Optical Model calculation (dotted curves), usual Coupled Channel calculation without considering the breakup channel (dashed curves), and full CDCC calculation (solid curves) carried out to describe the experimental inelastic scattering presented in this work (see text for details). This comparison has already been reported in Ref. [5] at eleven different bombarding energies. In this figure, only four energies (labeled in the laboratory frame) are shown.

in the analysis of the inelastic than for elastic scattering angular distributions. The present results show very clearly that inelastic scattering data are a useful tool to investigate the confidence of the calculations.

To see the relative contribution of each inelastic excitation to the summed inelastic angular distribution, we included in Fig. 4 their respective theoretical cross sections at three different bombarding energies. It can be seen that the quadrupole excitations contribute more at medium and forward angles and the octupole at the largest ones, and that the octupole cross sections increase with the energy.

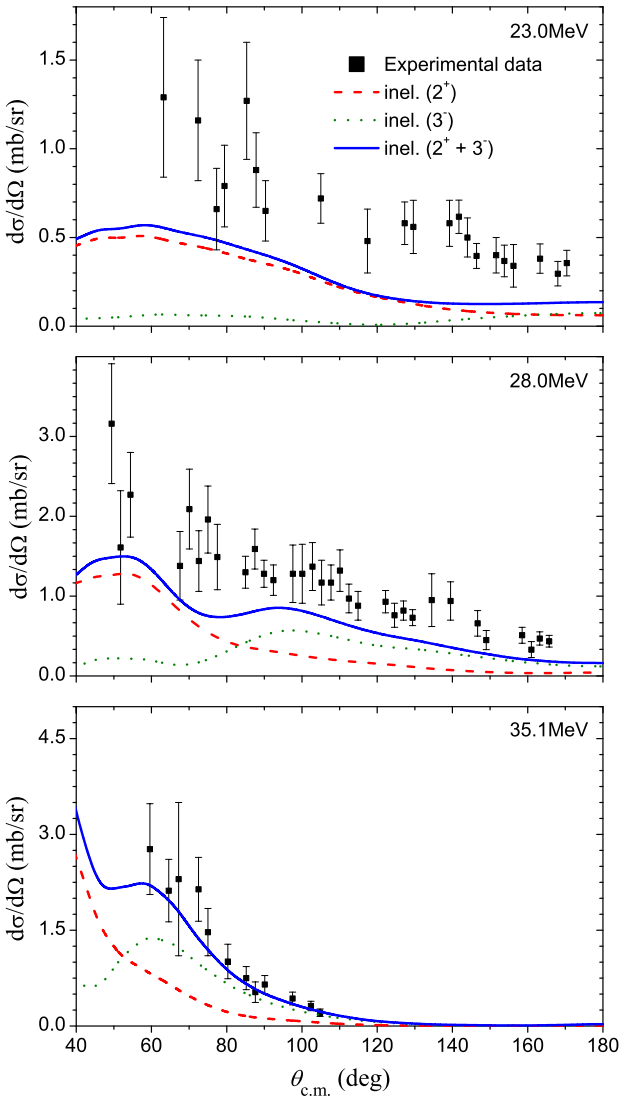

Fig. 4. (Color online.) Contribution of the 2_1^+ and 3_1^- target excitations (dashed and dotted curve, respectively) to the summed $(2_1^+ + 3_1^-)$ inelastic angular distribution (solid curve). The quadrupole excitations are more relevant at medium and forward angles and the octupole at the largest angles. The octupole cross sections increase with the energy. Only three energies (labeled in the laboratory frame) are shown.

Finally, we would like to show the sensitivity of our calculations to the optical potentials used in the calculations. Fig. 5 shows CDCC calculations for the elastic and inelastic scattering angular distributions at $E_{lab} = 30.1$ MeV, chosen as example. The full curves represent our previous calculations of Figs. 2 and 3. The dashed curves are the results using the SPP for the interaction α-deuteron to generate the bins. It can be seen that the results are very sensitive to the optical potential used. The reason for the disagreement may be that the double folding potential does not provide an adequate approximation of the interaction between these very light ions. The dotted

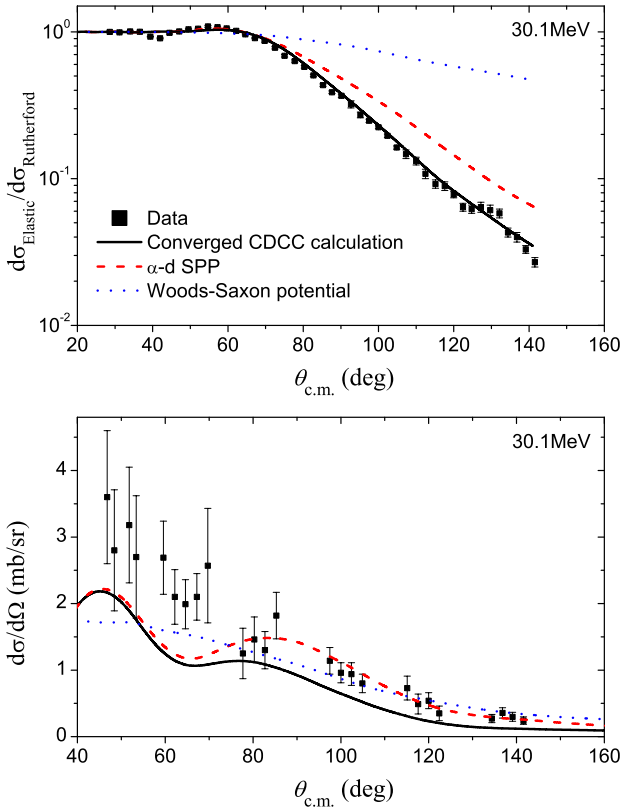

Fig. 5. (Color online.) Comparison of CDCC calculations using SPP and Woods–Saxon potentials at $E_{lab} = 30.1$ (see text for details).

curves are the results of a new CDCC calculation using the Woods–Saxon optical potential from systematics. For the real part of the ^{4}He + ^{144}Sm potential we used the one from Ref. [28] and for the deuteron + ^{144}Sm the one from Ref. [29]. The disagreement with the experimental data may be because we are using only the real part of the phenomenological effective optical potential of those systematics, which in principle depends on the imaginary part used to describe the elastic scattering angular distributions. In the case of the microscopic double folding potentials, they are derived from matter densities and the nucleon–nucleon interaction and they are independent of the imaginary part of the optical potential. These results show that in fact the double folding potential is more reliable for CDCC calculations than Woods–Saxon potentials, especially when all the relevant reaction channels are included in the coupling scheme.

5. Conclusions

We have reported angular distributions of original experimental inelastic scattering cross sections of the weakly bound ^{6}Li nucleus from a ^{144}Sm target (2_1^+ and 3_1^- target excited states) at seven bombarding energies near the Coulomb barrier. Those experimental results, together with pre-existent elastic scattering data, were used to determine the contribution of various channels involved in the ^{6}Li + ^{144}Sm reaction, by means of coupled channel and continuum discretized

coupled-channel calculations. The best agreement with the data was reached when a full CDCC calculation including continuum–continuum couplings was carried out. This result shows that when the breakup channel is present, one has to perform a full CDCC calculation that contains all important channels in the coupling scheme, including continuum–continuum couplings. At the lowest energies the calculations under-predict the experimental data by a factor of around two, although both experiment and theory agree in shape. The disagreement between the full CDCC calculations and the data at low energies can also be observed in the elastic scattering angular distributions (where the calculations over-predict the data), however the discrepancy is smaller than that observed in the inelastic scattering data. The effect of the continuum–continuum couplings on the calculated inelastic scattering angular distributions is negligible at near-barrier energies, but its importance increases dramatically for higher energies, where it increases the inelastic cross sections. We plan to elucidate possible sources of the discrepancies between full CDCC calculations and data by simultaneously analyzing the elastic and inelastic data for the $^{7}\mathrm{Li} + {}^{144}\mathrm{Sm}$ system.

Acknowledgements

The authors acknowledge the support of PROSUL-CNPq. D.R.O., J.L. and P.R.S.G. would like to thank CNPq, CAPES, FAPERJ and the PRONEX for their financial support. J.M.F., J.O.F.N. and P.R.S.G. thank CAPES-MYNCIT for their financial support.

References

[1] L.F. Canto, P.R.S. Gomes, R. Donangelo, M.S. Hussein, Phys. Rep. 424 (2006) 1.
[2] D.S. Monteiro, et al., Phys. Rev. C 79 (2009) 014601.
[3] D.R. Otomar, et al., Phys. Rev. C 80 (2009) 034614.
[4] J.M. Figueira, et al., Phys. Rev. C 81 (2010) 024613.
[5] D.R. Otomar, J. Lubian, P.R.S. Gomes, Eur. Phys. J. A 46 (2010) 285.
[6] D. Martinez Heimann, et al., AIP Conf. Proc. 1098 (2009) 275.
[7] D. Martinez Heimann, et al., AIP Conf. Proc. 1139 (2009) 11.
[8] M. Kamimura, M. Yahiro, Y. Iseri, Y. Sakuragi, H. Kameyama, M. Kawai, Prog. Theor. Phys. Suppl. 89 (1986) 1.
[9] N. Austern, Y. Iseri, M. Kamimura, M. Kawai, G. Rawitscher, M. Yahiro, Phys. Rep. 154 (1987) 125.
[10] Y. Sakuragi, M. Yahiro, M. Kamimura, Prog. Theor. Phys. 68 (1982) 322.
[11] N. Keeley, K. Rusek, Phys. Lett. B 357 (1996) 9.
[12] A. Diaz-Torres, I.J. Thompson, C. Beck, Phys. Rev. C 68 (2003) 044607.
[13] L.C. Chamon, D. Pereira, M.S. Hussein, M.A.C. Ribeiro, D. Galetti, Phys. Rev. Lett. 79 (1997) 5218.
[14] D. Abbott, et al., Eur. Phys. J. A 7 (2000) 421.
[15] A. Diaz-Torres, I.J. Thompson, Phys. Rev. C 65 (2002) 024606.
[16] S. Hashimoto, K. Ogata, S. Chiba, M. Yahiro, Prog. Theor. Phys. 122 (2009) 1291.
[17] T. Tamura, Rev. Mod. Phys. 37 (1965) 679.
[18] I.J. Thompson, Comput. Phys. Rep. 7 (1988) 3.
[19] M. Yahiro, et al., Prog. Theor. Phys. Suppl. 89 (1986) 32.
[20] N.C. Summers, F.M. Nunes, I.J. Thompson, Phys. Rev. C 74 (2006) 014606.
[21] S. Raman, C.W. Nestor Jr., P. Tikkanen, At. Data Nucl. Data Tables 78 (2001) 1.
[22] T. Kibedi, R.H. Spear, At. Data Nucl. Data Tables 80 (2002) 35.
[23] J. Lubian, et al., Phys. Rev. C 79 (2009) 064605.
[24] L.F. Canto, J. Lubian, P.R.S. Gomes, M.S. Hussein, Phys. Rev. C 80 (2009) 047601.
[25] S. Mukherjee, et al., Phys. Rev. C 80 (2009) 014607.
[26] C.J. Lin, et al., Nucl. Phys. A 787 (2007) 281.
[27] H.M. Jia, et al., Phys. Rev. C 82 (2010) 027602.
[28] F.B. Beccheti, G.W. Greenlees, Ann. Rep. of the J.H. Williams Lab. of Nucl. Phys., Univ. of Minnesota, 1969, p. 116.
[29] J.A.R. Griffith, M. Irshad, O. Karban, S. Roman, Nucl. Phys. A 146 (1970) 193.